Identification of Golgi-localized acyl transferases that palmitoylate and regulate endothelial nitric oxide synthase

Carlos Fernández-Hernando,[1] Masaki Fukata,[2,3] Pascal N. Bernatchez,[1] Yuko Fukata,[2] Michelle I. Lin,[1] David S. Bredt,[4] and William C. Sessa[1]

[1]Department of Pharmacology and Program in Vascular Cell Signaling and Therapeutics, Boyer Center for Molecular Medicine, Yale University School of Medicine, New Haven, CT 06536
[2]Laboratory of Genomics and Proteomics, National Institute for Longevity Sciences, Aichi 474-8522, Japan
[3]Precursory Research for Embryonic Science and Technology, Japan Science and Technology Agency, Kawaguchi, Saitama 332-0012, Japan
[4]Department of Integrative Biology, Eli Lilly and Company, Indianapolis, IN 46285

Lipid modifications mediate the subcellular localization and biological activity of many proteins, including endothelial nitric oxide synthase (eNOS). This enzyme resides on the cytoplasmic aspect of the Golgi apparatus and in caveolae and is dually acylated by both N-myristoylation and S-palmitoylation. Palmitoylation-deficient mutants of eNOS release less nitric oxide (NO). We identify enzymes that palmitoylate eNOS in vivo. Transfection of human embryonic kidney 293 cells with the complementary DNA (cDNA) for eNOS and 23 cDNA clones encoding the Asp-His-His-Cys motif (DHHC) palmitoyl transferase family members showed that five clones (2, 3, 7, 8, and 21) enhanced incorporation of [^{3}H]-palmitate into eNOS. Human endothelial cells express all five of these enzymes, which colocalize with eNOS in the Golgi and plasma membrane and interact with eNOS. Importantly, inhibition of DHHC-21 palmitoyl transferase, but not DHHC-3, in human endothelial cells reduces eNOS palmitoylation, eNOS targeting, and stimulated NO production. Collectively, our data describe five new Golgi-targeted DHHC enzymes in human endothelial cells and suggest a regulatory role of DHHC-21 in governing eNOS localization and function.

Introduction

The production of nitric oxide (NO) by the vascular endothelium is important for cardiovascular homeostasis, as endogenous NO regulates many fundamental cellular processes, including growth, mitochondrial respiration, differentiation, and migration. Endothelial NO synthase (eNOS or NOS3) synthesizes NO in the endothelium lining all blood vessels, and genetic deletion of eNOS causes many cardiovascular phenotypes, including increased blood pressure, impaired angiogenesis, abnormal vascular remodeling, and accelerated atherosclerosis (Fulton et al., 1999). eNOS is a peripheral membrane protein that is modified by dual acylation (N-myristoylation and S-palmitoylation), which targets it to specific biological membranes (Smotrys and Linder, 2004). All dually acylated proteins, including eNOS, src family members, and certain G-protein α subunits are cotranslationally N-myristoylated on cytoplasmic ribosomes followed by posttranslational cysteine palmitoylation. eNOS is N-myristoylated at glycine-2 and posttranslational S-palmitoylated on cysteines 15 and 26 (Sessa et al., 1993; Liu and Sessa, 1994; Liu et al., 1995; Robinson et al., 1995). N-myristoylation and S-palmitoylation mediate localization of eNOS to the Golgi complex and cholesterol-rich microdomains of the plasma membranes, including caveolae and lipid rafts (Garcia-Cardena et al., 1996; Shaul et al., 1996; Liu et al., 1997). Acylation-defective mutants of eNOS that cannot target either domain impair basal and agonist-stimulated NO release (Liu et al., 1995, 1996).

Little is known about the enzymatic mechanisms for dual palmitoylation in mammalian cells. This fatty acid modification is reversible, unlike N-myristoylation, which is permanent (Gordon et al., 1991). In the context of eNOS, palmitate turnover is 45 min, whereas myristate turnover occurs with the protein backbone (both ~20 h; Liu et al., 1995). Palmitoylation

Correspondence to William C. Sessa: william.sessa@yale.edu

Abbreviations used in this article: CRD, cysteine-rich domain; eNOS, endothelial NO synthase; HEK, human embryonic kidney; HUVEC, human umbilical vein endothelial cell; NO, nitric oxide; PAT, palmitoyl acyl transferase; WT, wild-type.

The online version of this article contains supplemental material.

The Journal of Cell Biology, Vol. 174, No. 3, July 31, 2006 369–377
http://www.jcb.org/cgi/doi/10.1083/jcb.200601051

and depalmitoylation of proteins may be regulated by extracellular signals, providing a mechanism for dynamic regulation of protein localization (James and Olson, 1989; Degtyarev et al., 1993; Mumby et al., 1994).

Recently, a new family of acyl transferase enzymes that catalyzed the protein palmitoylation was discovered (Fukata et al., 2004). Genetic screens in yeast identified Erf2/4 (Lobo et al., 2002) and Akr1p (Roth et al., 2002) as palmitoyl transferases for yeast Ras2 and casein kinase2 (Yck2). Deletion of Erf2/4 or Ark1 reduces palmitoylation of Ras2 or Yck2, respectively. Erf2/4 or Ark1 share a common region, the Asp-His-His-Cys motif (DHHC), within a cysteine-rich domain (CRD). The DHHC and CRD domains are essential for palmitoyl acyl transferase (PAT) activity (Roth et al., 2002; Fukata et al., 2004). The human homologues of the yeast Erf2–Erf4 complex are DHHC-9 and a Golgi-localized protein designated GCP16. This complex has been shown to palmitoylate H- and N-Ras in vitro (Swarthout et al., 2005). 23 genes encoding proteins with DHHC-CRD domains have been identified in mouse and human databases (Fukata et al., 2004). Some of these proteins are known as Golgi-specific DHHC zinc finger protein (GODZ/DHHC-3; Uemura et al., 2002), the c-Abl–associated protein Abl-philin2 (Aph2/DHHC-16; Li et al., 2002), Sertoli cell DHHC protein (SERZ-β/DHHC-7; Chaudhary and Skinner, 2002), Huntingtin interacting protein 14 (HIP14/DHHC-17; Huang et al., 2004), and DHHC-15, which palmitoylates the neuronal scaffold protein PSD-95 (Fukata et al., 2004).

In the present work, we screened the 23 known DHHCs to examine which isoforms can palmitoylate eNOS. We found that five mammalian DHHC proteins (DHHC-2, -3, -7, -8, and -21) palmitoylate eNOS, are present in human umbilical vein endothelial cells (HUVECs), and colocalize with eNOS on the Golgi apparatus. Finally, inhibition of DHHC-21 reduces eNOS palmitoylation, mislocalizes eNOS, and antagonizes NO release from endothelial cells.

Results

Identification of candidate eNOS PATs

Human embryonic kidney (HEK) 293 cells were cotransfected with each of the palmitoyl transferase cDNAs together with eNOS and the biosynthetic incorporation of ^{3}[H]-palmitate into eNOS examined by fluorography. As shown in Fig. 1 A, only five clones (DHHC-2, -3, -7, -8, and -21) markedly enhanced incorporation of ^{3}[H]-palmitate into eNOS (Fig. 1 A, top, see fold increase in label relative to total eNOS), defining them as putative eNOS PATs. The incorporation of palmitate into thioester linkages is sensitive to the strong base hydroxylamine. As shown in Fig. 1 B, the incorporation of ^{3}[H]-palmitate into eNOS is reduced by hydroxylamine, demonstrating that this occurs via a

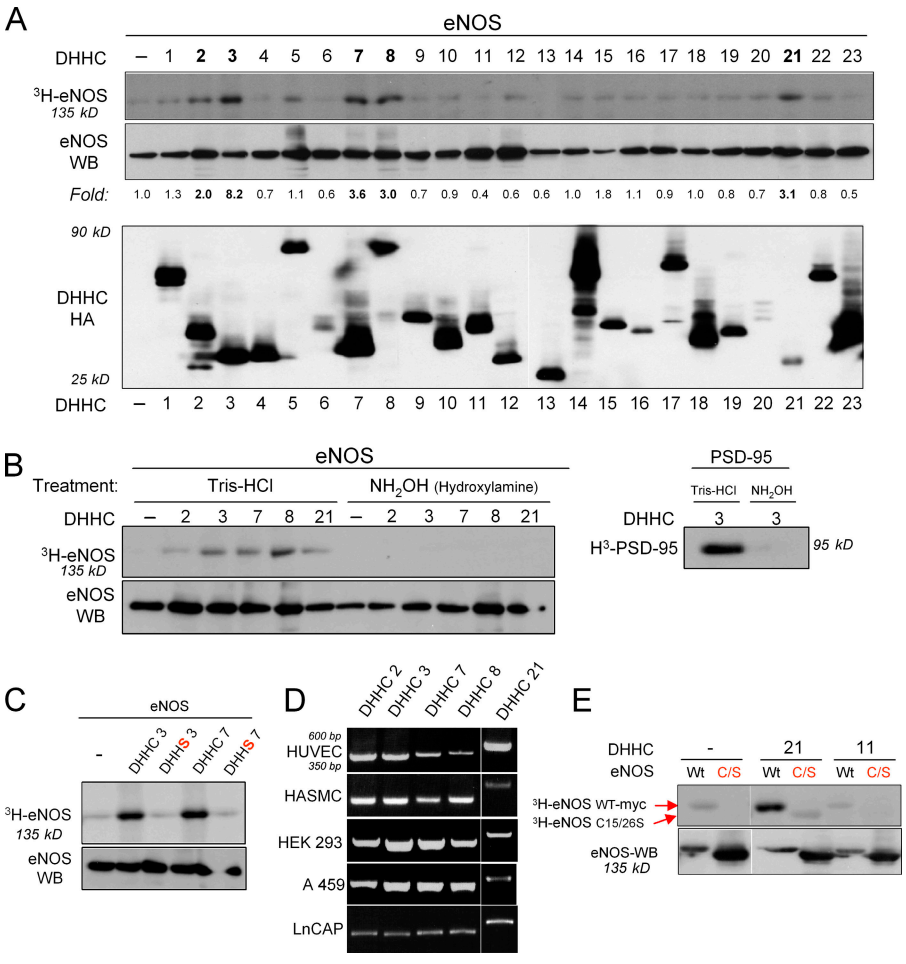

Figure 1. **Screening for potential eNOS PATs.** (A) Individual DHHC clones were cotransfected with eNOS into HEK 293 cells. After metabolic labeling with ^{3}[H]-palmitic acid, proteins were separated by SDS-PAGE, followed by fluorography (top; ^{3}[H]-eNOS). The same samples were analyzed by Western blotting (bottom; eNOS WB). Note that several DHHC enzymes enhance the incorporation of ^{3}[H]-palmitic acid into eNOS (bold numbers). The bottom blots depicts the level of the HA-tagged DHHC. (B) Treatment with hydroxylamine (NH_2OH) reduces ^{3}[H]-palmitate incorporation into eNOS after cotransfection of eNOS and several DHHC enzymes. The NH_2OH sensitivity of PSD-95 was used as control. (C) Mutagenesis of DHHC-3 and -7 abolishes the ^{3}[H]-palmitate incorporation into eNOS. (D) Total mRNA was isolated from different human cell lines, and the expression of DHHC isoforms was analyzed by RT-PCR. (E) The palmitoylation of WT eNOS by DHHC-21 is diminished by mutation of the two sites of eNOS palmitoylation, cysteines 15 and 26.

thioester linkage similar to the palmitoylation of PSD-95 by DHHC-3, which was recently described (Fukata et al., 2004). In addition, mutation in the core DHHC domain of these enzymes (mutation of DHHC to DHHS) reduces the incorporation of ^{3}[H]-palmitate into eNOS (Fig. 1 C), consistent with previous reports (Roth et al., 2002; Fukata et al., 2004). Next, we examined the expression of the five candidate eNOS PATs by RT-PCR in different human cell lines, including HUVECs, human aortic smooth muscle cells (HASMCs), HEK 293, lung carcinoma (A549), and prostate carcinoma cells (LnCAP). As shown in Fig. 1 D, all of tested DHHCs are expressed in the cell lines studied. However, in HUVEC, the major cell type that expresses eNOS, DHHC-21 was the most highly expressed, followed by DHHC-2 and -3. Cysteines 15 and 26 have been identified as the major sites of palmitoylation of eNOS (Liu et al., 1995; Robinson et al., 1995). As displayed in Fig. 1 E, transfection of DHHC-21, but not -11 (as a control), increases the incorporation of ^{3}[H]-palmitate into eNOS, an effect eliminated by mutation of cysteines 15 and 26 to serine (C15/26S eNOS).

DHHC-2, -3, -7, -8, and -21 localize to the Golgi region and plasma membrane in a pattern similar to eNOS

We expressed the HA-tagged DHHC proteins in COS-7 cells and localized them by immunofluorescence microscopy. As shown in Fig. 2 A, DHHC-21 (middle) colocalized with the Golgi matrix protein GM-130 (left), as did DHHC-2, -3, -7, and -8 (Fig. S1, available at http://www.jcb.org/cgi/content/full/jcb.200601051/DC1). Increasing the magnification of these images by 4× (Fig. 2 A, bottom) depicts clear colocalization of DHHC-21 with GM130 and a lesser amount of protein in the plasma membrane (Fig. 2 A, arrows). Next, we determined the proportional distribution of these enzymes in sodium carbonate using a discontinuous sucrose gradient. In this method, tightly embedded membrane proteins are buoyant (at the 5–30% sucrose interface in fractions 2–4), whereas soluble proteins remain at the bottom of the gradient (in fractions 7–10). In all the gradients, the distribution of caveolin-1, the coat protein of caveolae, and β-COP, a marker of Golgi and post-Golgi vesicles were used to confirm adequate fractionation. As shown in Fig. 2 B, the DHHCs and eNOS cofractionated into two pools, light membranes enriched in caveolin-1 and heavy membranes enriched in β-COP and β-actin (not depicted). Densitometric quantification (Fig. 2 B, right) of protein localization showed that a fraction of all DHHCs sediment as integral membrane proteins, with the greatest proportional amount for DHHC-2 and -21.

Colocalization and coimmunoprecipitation of DHHC enzymes with eNOS

Next, we examined colocalization of eNOS with DHHC enzymes by immunofluorescence microscopy in transfected cells. COS-7 cells were cotransfected with the cDNAs for eNOS and HA-tagged DHHC-21 and localized with antibodies against eNOS and the HA epitope. As shown in Fig. 3 A, eNOS and DHHC-21 (other DHHCs are shown in Fig. S2, available at http://www.jcb.org/cgi/content/full/jcb.200601051/DC1) colocalized in the Golgi region and to a lesser extent in plasma membrane.

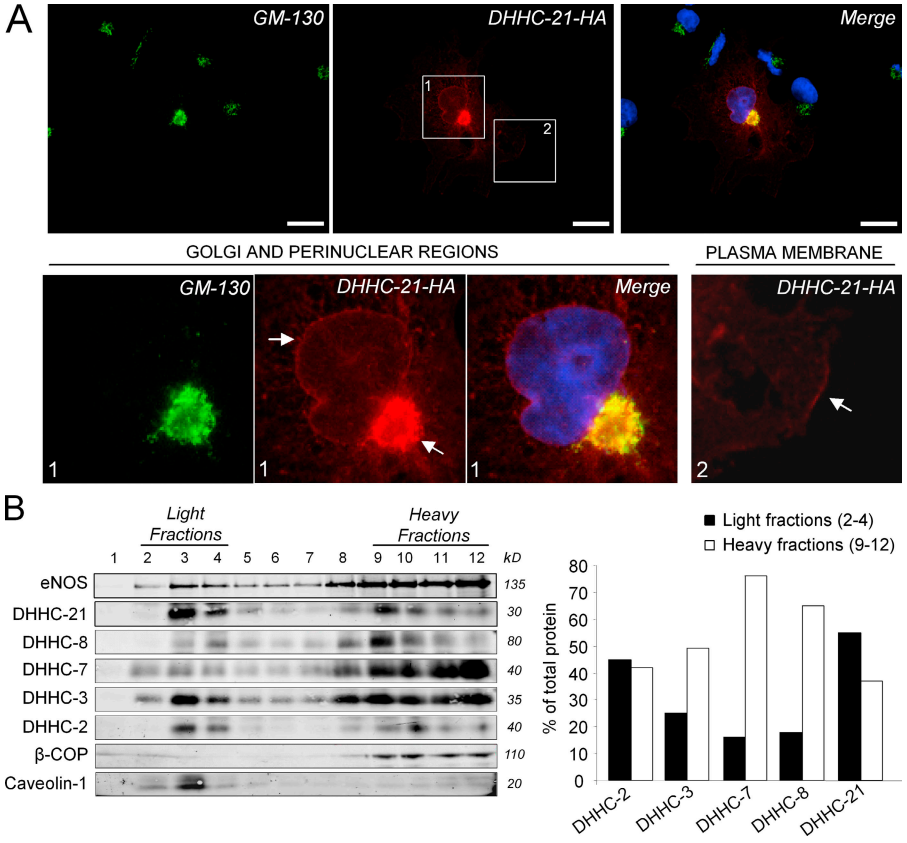

Figure 2. **DHHC-PATs colocalize with GM130 and eNOS and cosediment with eNOS.** (A) COS-7 cells were transfected with HA-tagged DHHC cDNAs. After 48 h, cells were fixed, incubated with antibodies against GM-130 (Golgi marker; green) and HA (red), and mounted on glass slides with medium containing nuclear dye DAPI (blue). Merged images with DAPI are shown. Bars, 10 μm. (B) COS-7 cells were transfected with plasmids encoding DHHC-HA enzymes and eNOS, and lysates were fractionated as described (see Materials and methods). Equal volumes of each fraction were separated by SDS-PAGE and Western blotted for eNOS, HA, caveolin-1, and β-COP. Results are representative of two separate experiments that gave similar results. Quantitative analysis shows that DHHC-2 and -21 are enriched in light membrane fractions. In region of interest 1, the arrow is pointing to Golgi-localized DHHC-21, whereas in region of interest 2, the arrow is pointing to DHHC-21 in plasma membrane.

Because palmitoylation is a cytoplasmic event and eNOS is a peripheral membrane protein, we determined whether DHHC enzymes and eNOS can interact. As seen in Fig. 3 B (left), the HA-tagged DHHCs and eNOS were well expressed in total cell lysates prepared from the cells. Immunoprecipitation of HA-tagged DHHC enzymes using an anti-HA monoclonal antibody detected the coassociation with eNOS (Fig. 3 B, right, third to seventh lanes) with the DHHCs, whereas no immunoreactive protein was observed after immunoprecipitation of lysates from cells expressing eNOS alone (Fig. 3 B, right, first lane).

Previously, we targeted eNOS to the Golgi versus the plasma membrane using different domains of syntaxin-3 (Fulton et al., 2004; Jagnandan et al., 2005). To determine the importance of localization on the interaction between eNOS and DHHC enzymes, we cotransfected Golgi-targeted eNOS (eNOS S17) or plasma membrane–targeted eNOS (eNOS S25) and DHHC-3, -7, and -21. As shown in Fig. 3 C, the interaction between the Golgi-targeted eNOS and the DHHC enzymes was stronger than the plasma membrane–targeted isoform, consistent with the majority of DHHCs and eNOS present on the Golgi of transfected cells (Fig. 2).

Next, we assessed whether the phosphorylation state could affect the interaction of eNOS with DHHCs. To address this question, DHHCs were cotransfected with wild-type (WT) eNOS and two eNOS phosphomutants, eNOS S1179A and S1179D. Serine 1179 is a key phosphorylation site for several kinases, including Akt, AMP kinase, and cAMP protein kinase (Fulton et al., 2001), and phosphorylation of this site is associated with eNOS activation. Mutation of S1179 to D renders eNOS constitutively active, whereas S1179 to A is less activated (Dimmeler et al., 1999; Fulton et al., 1999; McCabe et al., 2000). As seen in Fig. 3 D, in all cases, WT and phosphomutants were associated with DHHC enzymes, indicating that phosphorylation of this particular residue was not critical for the interaction of eNOS with DHHC-3 and -21.

eNOS fatty acylation is required for an efficient interaction with DHHC proteins and NO release

To examine whether the localization of eNOS is important for the interaction of eNOS with DHHCs, COS cells were transfected with WT and different mutants of eNOS that influence eNOS acylation and targeting (Fig. 4 A). Cells were transfected with WT eNOS (N-myristoylated and S-palmitoylated, Golgi, and plasmalemma targeted), G2A eNOS (neither N-myristoylated nor S-palmitoylated and cytosolic), C15/26S eNOS (N-myristoylated but not S-palmitoylated; diffuse perinuclear localization), or L2S eNOS (N-myristoylated but not palmitoylated because of the mutation of the intervening leucines between the two palmitoylation sites, C15 and C26;

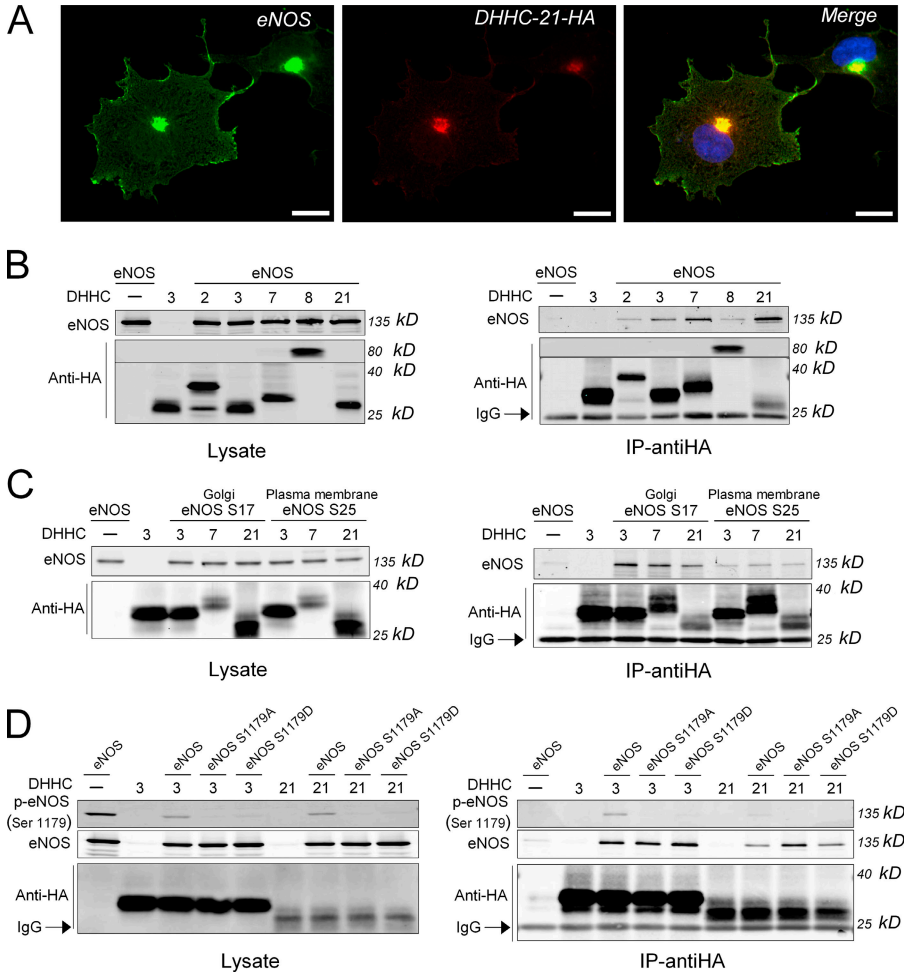

Figure 3. **DHHC-PATs colocalize with eNOS and interact in coprecipitation experiments.** (A) COS-7 cells were transfected with eNOS and HA-tagged DHHC-21 cDNAs. After 48 h, cells were fixed, incubated with antibodies against eNOS (green) and HA (red), and mounted on glass slides with medium containing nuclear dye DAPI (blue). Bars, 10 µm. (B) Coexpression of eNOS and DHHCs in COS-7 cell lysates (left) and the interaction between eNOS and the DHHC-HA after purification of the HA-tagged DHHC (right). (C) Coexpression of Golgi-targeted eNOS (S17 eNOS) or plasma membrane–targeted eNOS (S25 eNOS) and DHHCs in COS-7 cell lysates (left) and the coprecipitation of eNOS isoforms with DHHC-HA enzymes (right). (D) WT and eNOS phosphomutants (S1179A and S1179D eNOS) and DHHC-PATs were coexpressed in COS-7 cells (left), and the interaction between these proteins was studied after immunoprecipitation using anti-HA antibody (right). These experiments are representative of three separate experiments that gave similar results.

diffuse perinuclear pattern; Liu et al., 1995, 1997; Sessa et al., 1995) with DHHC-3–HA. As shown in Fig. 4 B (left), WT eNOS is primarily Golgi targeted and G2A eNOS is diffusely distributed throughout the cells, whereas the palmitoylation-deficient mutants, C15/26S and L2S eNOS, were retained in the perinuclear region but are more diffusely distributed compared with WT eNOS. WT eNOS clearly colocalized with HA-tagged DHHC-3, whereas G2A eNOS did not, and the palmitoylation mutants (C15/26S and L2S eNOS) had a partially overlapping perinuclear pattern.

Next, we performed coimmunoprecipitation experiments to determine the role of acylation and subcellular localization on the coassociation of eNOS with DHHC. The eNOS constructs and DHHC-3 or -21 were equally expressed based on Western blotting of the proteins in cell lysates (Fig. 4 C, left), and immunoprecipitation of DHHC-3–HA resulted in ample recovery (Fig. 4 C, middle) of DHHC-3 and -21. Interestingly, immunoprecipitation of DHHC-3 and -21 resulted in the coassociation with WT eNOS but not with the other acylation-defective eNOS mutants (Fig. 4 C, right). These results indicate that the fatty acylation and targeting are important for the interaction between eNOS and the DHHC-PATs.

Finally, we examined whether the DHHCs can influence eNOS function by measuring NO release (as nitrite after 24 h of accumulation). Cotransfection of COS-7 cells with WT eNOS and DHHC-3, -7, and -21 increased the basal accumulation of NO_2^- into the media (Fig. 4 D). However, this effect was eliminated in cells cotransfected with acylation-defective G2A or C15/26S eNOS (Fig. 4, E and F).

Knock down of endogenous DHHC-21, but not -3, levels in endothelial cells impairs eNOS palmitoylation, cellular targeting, and NO release

Although several DHHC enzymes can palmitoylate eNOS, DHHC-21 mRNA was the most highly expressed in endothelial

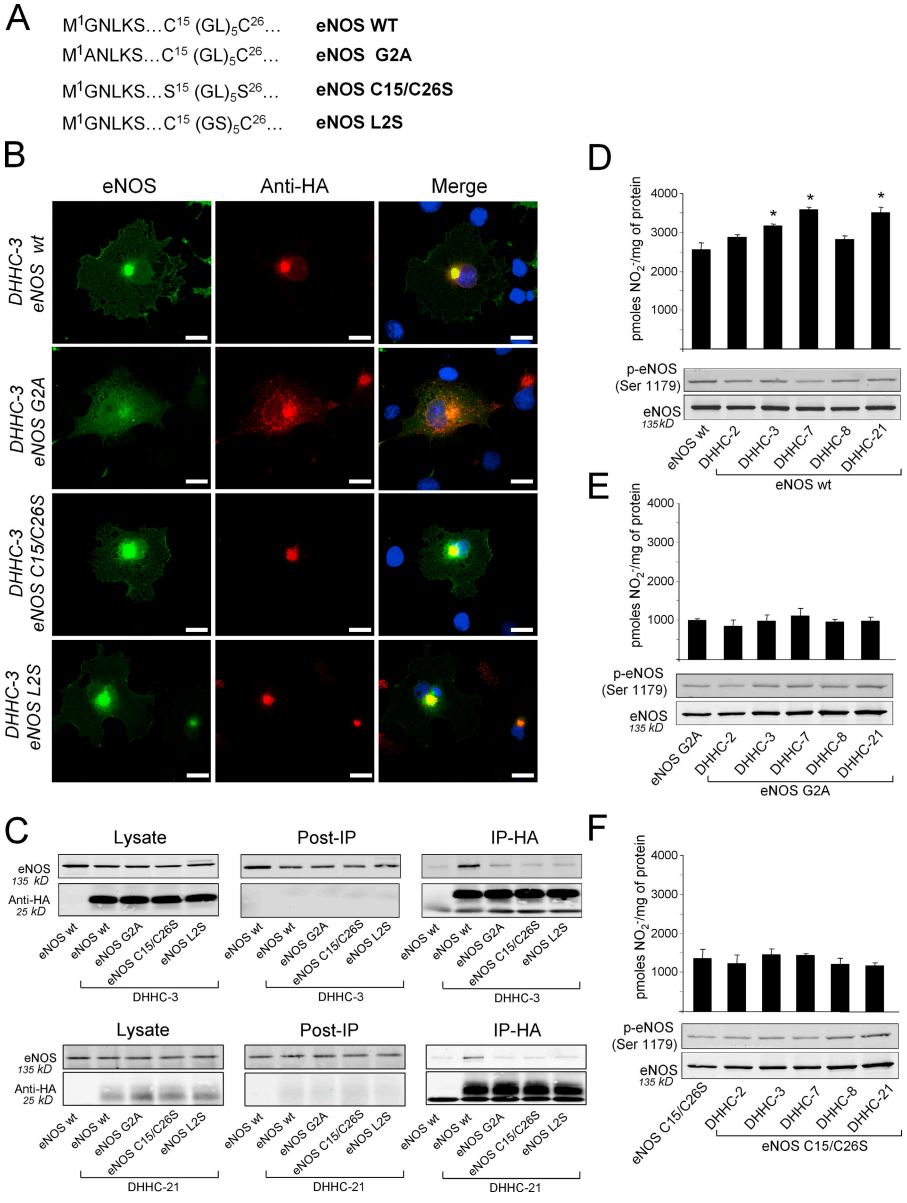

Figure 4. **eNOS palmitoylation state regulates the interaction of eNOS with DHHC-PATs and NO release.** (A) Schematic illustration of eNOS constructs. WT eNOS (both myristoylated and palmitoylated), G2A eNOS (neither myristoylated nor palmitoylated), and C15/26S and L2S eNOS (myristoylated but not palmitoylated). (B) COS-7 cells were transfected with HA-tagged DHHC and eNOS cDNAs. After 48 h, cells were fixed, incubated with antibodies against eNOS (green) and HA (red), and mounted on glass slides with medium containing nuclear dye DAPI (blue). Merged images with DAPI are shown. Bars, 10 μM. (C) COS-7 cells transfected with plasmids encoding DHHC-3 (top) or -21 (bottom) and eNOS mutants were subjected to immunoprecipitation with anti-HA monoclonal antibody and Western blotted for eNOS to determine relative coassociation with DHHC enzymes. The left panels show expression of eNOS (top) and DHHC-PPATs (bottom) in total cell lysates, the middle panels show the quantitative recovery of the HA-tagged DHHC, and the right panels show the specific coassociation of WT eNOS with DHHC-3 and -21. The Western blots are representative of two separate experiments that gave similar results. NO release from COS-7 cells cotransfected with WT eNOS (D), G2A eNOS (E), C15/C26 eNOS (F), and DHHC (D–F) cDNAs. The nitrite accumulation in the medium was quantified after 24 h. All of the data represent the mean ± SEM in three separate experiments. *, $P < 0.05$ compared with eNOS alone.

cells, and the protein localized on the Golgi and interacted with eNOS. To determine the role of DHHC-21 in palmitoylating eNOS in endothelial cells, an RNAi approach was used. As shown in Fig. 5 A, transfection of endothelial cells with DHHC-21 siRNA duplex RNAs (at 12.5 nM) reduced the expression of DHHC-21 (via quantitative RT-PCR) expression in a time-dependent manner, with maximal reduction at 48 h, where nonsilencing RNA as a control was ineffective. The reduction in DHHC-21 mRNA levels resulted in a marked diminution in the incorporation of ^{3}[H]-palmitate into eNOS by ~60% (Fig. 5 B). Because eNOS palmitoylation is crucial for the perinuclear targeting of eNOS onto the Golgi, we performed an immunofluorescence analysis of eNOS in DHHC-21–depleted endothelial cells. As shown in Fig. 5 C (middle), knock down of DHHC-21 resulted in a more diffuse, perinuclear pattern of eNOS immunoreactivity compared with cells treated with nonsilencing RNA (left). In addition, treatment of endothelial cells with 2-bromopalmitate, a substrate-based inhibitor of palmitoylation, resulted in a similar but more extensive mislocalization of eNOS (Fig. 5 C, right).

We next examined the effect of DHHC-21 knockdown on basal and agonist-stimulated NO release from endothelial cells. In endothelial cells, increases in cytoplasmic calcium activate calmodulin, which binds to the canonical CaM binding domain in eNOS and serves as an allosteric regulator of electron flux through eNOS, leading to a burst of NO release (Busse and Mulsch, 1990; Pollock et al., 1991; Fulton et al., 2001). Reduction of DHHC-21, but not treatment with nonsilencing RNA, caused a slight decrease the basal accumulation of NO_2^- into the media (Fig. 4 D, left). More important, reduction in DHHC-21 reduced the release of NO_2^- stimulated by both ionomycin (middle) and ATP (right), indicating the importance of eNOS palmitoylation via DHHC-21 for eNOS activation. To examine the specificity of DHHC-21 knockdown on eNOS function, we also reduced the levels of DHHC-3 with RNAi. As seen in Fig. 5 E, transfection of endothelial cells with DHHC-3 siRNA (at 12.5 nM) reduced the expression of DHHC-3 (via quantitative RT-PCR) expression where nonsilencing RNA as a control was ineffective. However, under these conditions, basal and ATP-stimulated NO_2^- was not affected (Fig. 5 F).

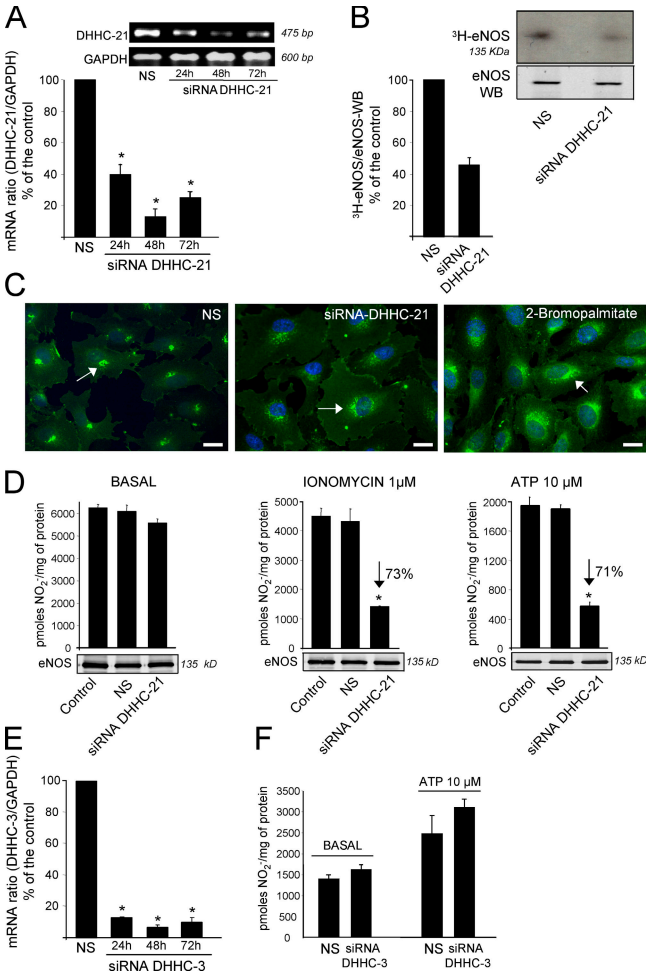

Figure 5. **Depletion of DHHC-21 expression in endothelial cells reduces eNOS palmitoylation, localization, and NO release.** (A) DHHC-21 siRNA down-regulates DHHC-21 mRNA expression. EA.hy.926 cells were transfected with a control (nonsilencing [NS]) or DHHC-21 siRNA duplex. The DHHC-21 expression at the indicated time points was determined by real-time PCR. (B) EA.hy.926 cells were transfected with a control (nonsilencing) or DHHC-21 siRNA, and cells were labeled with ^{3}[H]-palmitate for 4 h and eNOS immunoprecipitated. The percentage of labeled eNOS/total eNOS from two experiments was then quantified. (C) EA.hy.926 cells were transfected with nonsilencing or DHHC-21 siRNA or treated with 100 μM 2-bromopalmitate, and cells were fixed and stained for eNOS (green) and nuclei (DAPI; blue) and analyzed by immunofluorescence microscopy. Arrows indicate a significant decrease in NO_2^- release after DHHC-21 knockdown. Bars, 15 μm. (D) NO release from control EA.hy.926 cells or cells transfected with nonsilencing or DHHC-21 siRNAs. The nitrite accumulation was quantified for 8 h (basal; left) and after the stimulation with ionomycin (middle) or ATP (right) for 30 min. (E) DHHC-3 siRNA down-regulates DHHC-3 mRNA expression. EA.hy.926 cells were transfected with a control (nonsilencing) or DHHC-3 siRNA duplex. The DHHC-3 expression at the indicated time points was determined by real-time PCR. (F) NO release from control EA.hy.926 cells or cells transfected with nonsilencing or DHHC-3 siRNAs. The nitrite accumulation was quantified for 8 h (basal) and after the stimulation with ATP for 30 min. The data represent the mean ± SEM of triplicate samples repeated in three separate experiments. *, $P < 0.05$ compared with control.

Discussion

The most salient feature of this paper is the identification of five DHHC-PAT cDNAs that can palmitoylate the dually acylated, peripheral membrane protein eNOS in vivo. DHHC-2, -3, -7, -8, and -21 colocalize with GM-130, a peripheral membrane protein of the Golgi in transfected cells, suggesting that palmitoylation can occur on the cytoplasmic aspect of the Golgi complex. The aforementioned DHHC-PATs also colocalize and associate with eNOS, providing evidence for the compartmentalization of protein palmitoylation. Most critical, reduction of DHHC-21 in endothelial cells diminishes eNOS palmitoylation, mislocalizes eNOS, and impairs agonist-stimulated NO release.

Although cysteine palmitoylation has long been recognized as important for protein trafficking and function, enzymes responsible for this have been elusive. Genetic and biochemical studies in yeast initially identified that two genes containing CRDs are essential for palmitoylation of Ras2 and casein kinase (Lobo et al., 2002; Roth et al., 2002). This led to the discovery of mammalian DHHC genes and identification of their specific substrates. Out of the 23 independent mammalian genes encoding

DHHC-containing proteins, only a few enzyme substrates have been identified. DHHC-2, -3, -7, and -15 can palmitoylate PSD-95 (Fukata et al., 2004), DHHC-3 (GODZ; Uemura et al., 2002) can palmitoylate the GABA-A receptor (Keller et al., 2004), DHHC-17 can palmitoylate several neuronal substrates, including SNAP-25 and PSD-95 (Huang et al., 2004), and DHHC-9 can palmitoylate H- and N-Ras (Swarthout et al., 2005). In the present study, only DHHC-2, -3, -7, -8, and -21 significantly increased the incorporation of palmitate into eNOS, suggesting some degree of substrate specificity of the DHHCs. As DHHC-2, -3, and -7 can palmitoylate the nonmyristoylated proteins PSD95 and GαS, these candidates are less likely to be specific N-myristoyl–requiring PATs (Fukata et al., 2004). RNAi-mediated knockdown of endogenous DHHC-21 in endothelial cells reduces the incorporation of ^{3}[H]-palmitate into eNOS, mislocalizes eNOS, and reduces agonist-stimulated NO release, whereas knock down of DHHC-3 did not reduce NO release, suggesting that although at least five DHHCs can significantly palmitoylate eNOS in transfected cells, DHHC-21 may be a more specific eNOS PAT. The reasons for the apparent specificity of DHHC-21 toward eNOS in endothelial cells are not known, but it may be due to the amount of DHHC-21 protein relative to other DHHCs expressed in endothelial cells or to the posttranslational modification of DHHCs that may determine its substrate specificity or regulate its activity in a cell-specific context. In addition, we cannot rule the possibility that other DHHCs palmitoylate eNOS in endothelial cells, as a substantial knock down of DHHC-21 reduced palmitoylation by only 50% and NO release by 70%. Additional experiments using isoform-selective antibodies and recombinant DHHC proteins with various substrates will help deconvolve DHHC substrate specificity and kinetics in more detail.

Other interesting findings are that DHHC-2, -3, -7, -8, and -21 all enhance the transfer of palmitate into eNOS and are strongly colocalized with GM130, a Golgi matrix protein localized to the cytoplasmic face of the Golgi, consistent with our previous suggestion that the Golgi is the site for eNOS palmitoylation (Garcia-Cardena et al., 1996). Palmitoylation of substrates on the Golgi would stabilize protein association via kinetic trapping (Sowa et al., 1999) and allow for protein localization either on the Golgi or movement to the plasma membrane, as recently confirmed for Ras (Rocks et al., 2005). Supporting this are data showing that DHHC-9, an H- and N-Ras PAT, colocalizes and interacts with GCP16, which is a Golgi-localized cosubunit (Swarthout et al., 2005) that appears necessary for DHHC-9 activity toward Ras and movement of Ras to the plasma membrane.

For most dually acylated proteins, N-myristoylation is a cotranslational modification that favors posttranslational cysteine palmitoylation. For eNOS, mutation of the palmitoylation sites does not affect N-myristoylation but blocks tight perinuclear targeting and NO release from cells (Liu et al., 1995, 1996, 1997). The mistargeting and dysfunction of these mutants may reflect a structural change or lack of palmitoylation; however, our RNAi experiments, which show that reduction in DHHC-21 decreases eNOS palmitoylation and impairs targeting, indicate that palmitoylation of eNOS is crucial for proper targeting and function.

The discovery of DHHC-PATs in vascular cells represents a new, exciting area. Many proteins involved in signal transduction are palmitoylated, and this fatty acid modification is often necessary for function. Understanding the tissue and cellular distribution of DHHCs and their substrates is critical for identification of PAT inhibitors that may be therapeutically useful. Our data showing that DHHC-21 is a major eNOS PAT suggests that antagonizing this enzyme may be useful for reducing NO-dependent changes in vascular permeability and tumor angiogenesis.

Materials and methods

Chemicals and antibodies

Mouse monoclonal antibodies against caveolin-1, GM 130, and eNOS were provided by BD Biosciences. Rabbit polyclonal antibody anti–β-COP was purchased from Affinity BioReagents, Inc. Mouse monoclonal against β-actin antibody was provided by Sigma-Aldrich. Rat monoclonal antibody anti-HA high affinity (3F10) was purchased from Roche. Rabbit polyclonal antibody against phospho-eNOS (Ser 1179) was obtained from Zymed Laboratories. Goat anti–mouse IRDye 800–conjugated antibody was purchased from Rockland. Goat anti–rabbit Alexa fluor 680 antibody was provided by Invitrogen, and goat anti–rat Texas red dye–conjugated antibody was purchased from Jackson ImmunoResearch Laboratories. The chemical products were provided by Sigma-Aldrich.

Cell culture

HEK 293, COS-7, HASMC, A 459, LnCap, and EA.hy.926 cells were grown in high-glucose DME (Invitrogen) supplemented with FBS (Hyclone), penicillin-streptomycin (Sigma-Aldrich), and HAT (EA.hy.926 only; Sigma-Aldrich) at 37°C in a humidified atmosphere of 5% CO_2. HUVECs were grown in EGM-2 media (Clonetics).

Plasmid constructions and cell transfections

cDNAs encoding DHHC proteins were cloned in PEF-Bos-HA (BD Biosciences) as previously described (Fukata et al., 2004). WT, C15/26S, G2A, and L2S eNOS cDNAs were constructed and subcloned into the mammalian expression vector pcDNA3 (Invitrogen) as previously described (Liu et al., 1997). S17, S25, S1179A, and S1179D eNOS cDNAs were constructed and subcloned in pcDNA3 vector (Invitrogen) as previously described (Fulton et al., 1999, 2004; Jagnandan et al., 2005). The sequences of the PCR fragments cloned were verified by DNA sequencing. For cell transfection, semiconfluent (60%) COS-7 and HEK 293 cells were grown in 6-well plates and transfected with the different plasmids using Lipofectamine 2000. A β-gal plasmid was used to normalize DNA quantities.

Immunofluorescence

COS-7 and EA.hy.926 cells grown on coverslips were fixed with 4% PFA for 5 min at room temperature and rinsed twice with PBS. The cells were then permeabilized with 0.1% Triton X-100 for 10 min, washed twice with PBS, and incubated with blocking solution (5% normal goat serum in PBS) for 45 min at room temperature. Next, the cells were incubated with the primary antibodies (diluted 1:500) overnight at 4°C and washed twice with blocking solution, followed by a 45-min incubation with fluorophore-conjugated secondary antibody (FITC or TRITC; diluted 1:250) at room temperature. The coverslips were then mounted on glass slides with Gelvatol/DAPI (Sigma-Aldrich) and analyzed with an epifluorescence microscope (Axiovert; Carl Zeiss MicroImaging, Inc.) with a 63× objective. Images were acquired using a charge-coupled device camera (Axio; Carl Zeiss MicroImaging, Inc.). Analysis of different images was performed using Openlab software (Improvision) after subtracting background.

NO release analysis

48 h after transfection of eNOS and DHHC plasmids into COS-7 cells, the media was removed and the cells were supplemented with serum-free DME for 24 h. The media was then processed for the measurement of nitrite (NO_2^-) by a NO-specific chemiluminescence analyzer (Sievers) as described previously (Fulton et al., 1999). The same cells were then incubated with fresh, serum-free DME for 30 min to calculate the preagonist nitrite accumulation. Subsequently, the cells were incubated with 1 μM ionomicin for another 30 min to allow postagonist nitrite accumulation.

The medium was then harvested, and nitrite accumulation was measured. In other experiments, DHHC-21 and -3 were silenced after treatment with specific siRNAs for 48 h, and EA.hy.926 cells were analyzed for basal and stimulated NO release as described.

Sucrose gradient

Transfected COS-7 cells (150-mm dish) were washed twice with PBS and scrapped into 2 ml of ice-cold 500 mM sodium carbonate, pH 11, supplemented with 1 mg/ml protease inhibitor cocktail (Roche), Dounce homogenized, and sonicated (three 20-s bursts at 30% of maximal power). The homogenate was then adjusted to 42.5% sucrose by the addition of 2 ml 85% sucrose prepared in MBS (25 mM MES, pH 6.5, and 0.5 M NaCl) and placed at the bottom of an ultracentrifuge tube. A 5–30% discontinuous sucrose gradient was formed (3 ml of 5% sucrose and 5 ml of 30% sucrose, both in MES containing 250 mM sodium carbonate) and centrifuged at 35,000 rpm for 18 h in a rotor (SW40; Beckman Coulter). Gradient fractions (1 ml) were collected from the top of the tube, and 50 μl of each fraction (1–12) was used for Western blotting analysis as described previously (Sowa et al., 1999). The percentage of total proteins in different fractions was determined by densitometry and plotted as percentage of total protein (NIH program).

Immunoprecipitation and immunoblotting

EA.hy.926 and COS-7 cells were lysed in ice-cold buffer containing 50 mM Tris-HCl, pH 7.5, 10% glycerol, 125 mM NaCl, 1% NP-40, 5.3 mM NaF, 1.5 mM NaP, 1mM orthovanadate, 1 mg/ml protease inhibitor cocktail (Roche), and 0.25 mg/ml AEBSF (Roche). Cell lysates were rotated at 4°C for 30 min before the insoluble material was removed by centrifugation at 12,000 *g* for 10 min. After normalizing for equal protein concentration, lysates were precleared by incubation with protein G–agarose for 45 min at 4°C with rocking. Precleared samples were then immunoprecipitated with anti-HA and anti-eNOS antibodies. Proteins in both the cell lysates and immunoprecipitates were heated in SDS sample buffer before separation by SDS-PAGE. After overnight transfer of the proteins onto nitrocellulose membranes, Western blots were performed using the antibodies described above (see Chemicals and antibodies).

Palmitate labeling

Transfected HEK 293 cells were preincubated for 30 min in serum-free DME with 10 mg/ml of fatty acid–free BSA (Sigma-Aldrich). Cells were then labeled with 0.5 mCi/ml ^{3}[H]-palmitic acid (PerkinElmer) for 4 h in the preincubation medium. Cells were washed with PBS, scraped with SDS-PAGE sample buffer (62.5 mM Tris-HCl, pH 6.8, 10% glycerol, 2% SDS, 0,001% bromophenol blue, and 10 mM DTT), and boiled for 2 min. In other experiments, EA.hy.926 cells were solubilized by incubation in 1 ml of lysis buffer containing 50 mM Tris-HCl, pH 7.5, 10% glycerol, 125 mM NaCl, 1% NP-40, 5.3 mM NaF, 1.5 mM NaP, 1 mM orthovanadate, 1 mg/ml protease inhibitor cocktail, and 0.25 mg/ml AEBSF and subjected to eNOS immunoprecipitation as described above (see Immunoprecipitation and immunoblotting). For fluorography, protein samples were separated by SDS-PAGE. Gels were treated with Amplify (GE Healthcare) for 30 min, dried under vacuum, and exposed to a film (Biomax MS; Kodak). Autoradiographs were scanned with a scanner (Canon) and quantified using the IMAGE J (NIH) program.

siRNA treatment

DHHC-21 (available from GenBank/EMBL/DDBJ under accession no. NM_178566) DNA and DHHC-3 (accession no. NM_016598) target sequences were designed by QIAGEN (HP guaranteed siRNA). In all experiments, we used the same concentration of each of the four siRNAs (12.5 nM). The target sequences for DHHC-21 were 5′-CAGGCAGTTATAAGATTGCAA-3′ (siRNA-1), 5′-CTAGTATAACTAGATAGTATA-3′ (siRNA-2), 5′-TAGCTAGTGTTAGGAAGTGAA-3′ (siRNA-3), and 5′-CACCTTCTTATAGTATAGGTA-3′ (siRNA-4). The target sequences for DHHC-3 were 5′-ACGGGAATAGAACAATTGAAA-3′ (siRNA-1), 5′AACATTGAGCGGAAACCAGAA-3′ (siRNA-2), 5′-AAAGGAAATGCCACTAAAGAA-3′ (siRNA-3), and 5′-CTACGTGTATAGCATCATCAA (siRNA-4). Our nonsilencing DNA target was 5′-AATTCTCCGAACGTGTCACGT-3′. siRNA duplexes were formed according to the manufacturer's protocol. For cell transfection, EA.hy.926 cells were grown to 30% of confluence in 6-well plates. 150 μl of Opti-MEM-1 medium (Invitrogen) was incubated for 5 min with siRNA sequences (50 nM final concentration). In addition, 150 μl of Opti-MEM-1 was incubated with 5 μl of Oligofectamine (Invitrogen) for 5 min. The two solutions were combined and incubated at room temperature for 30 min and then added to cells (1.5 ml of total volume) for 6 h. After transfection, cells were supplemented with 1.5 ml of DME with 10% FBS and antibiotics.

RT-PCR and quantitative real-time PCR

Total RNA was extracted with Trizol reagent (Invitrogen). cDNA was synthesized from 5 μg using SuperScript first-strand synthesis system for RT-PCR (Invitrogen). A 1-μl aliquot of the reverse-transcription reaction was then used for subsequent PCR amplification with specific primers. Each 25-μl PCR contained 1 μl of the reverse-transcription reaction, 1 mM dNTPs (Roche), 20 pmol of each primer, and 1.25 U of *Taq* DNA polymerase (QIAGEN). The primers sequences used were as follows: GAPDH (available from GenBank/EMBL/DDBJ under accession no. BC_013310),5′-CCACCCATGGCCAAATTCCATGGCA-3′and5′-TCTAGACGGCAGGTCAGGTCCACC-3′; DHHC-2 (accession no. NM_016353), 5′-CGCCATCCAGCTGTGCATAGTG-3′ and 5′-GAGCAGTGATGGCAGCGATCTG-3′; DHHC-3 (accession no. NM_016598), 5′-TGTTTGTAAGCGGTGCATTCGG-3′ and 5′-TTGGTCTGGCGTGGCAAAGG-3′; DHHC-7 (accession no. NM_017740), 5′-TGCGATGGGAAGGGATGAAGTC-3′ and 5′-GGCGTTTGGCTTCTTCGTGTG -3′; DHHC-8 (accession no. NM_013373), 5′-TCAAACCCGCCAAGTACATCCC-3′ and 5′-ACGCCCGATGCAGTTGTTGAC-3′; and DHHC-21 (accession no. NM_178566) 5′-AAGCGTTCCCATCACTGCAGC-3 ′and 5′-GAACTCGCAGTGGTTGCCTCTG-3′. Each cycle of PCR consisted of denaturation at 90°C for 1 min, primer annealing at 60°C for 1 min, and primer extension at 72°C for 2 min. PCR products were separated on a 2% agarose gel and stained with ethidium bromide. Quantitative real-time PCR was performed by using iQ SYBR green supermix on iCycler real-time detection system (Bio-Rad Laboratories).

Statistical analysis

The results are expressed as mean ± SD. Statistical comparisons between groups were done by the *t* test, using the Statgraphics Plus 5.0 program (Statistical Graphics Corp.).

Online supplemental material

Fig. S1 shows the colocalization between DHHC-CRD enzymes (DHHC-2, -3, -7, and -8) and GM-130, a Golgi marker. Fig. S2 demonstrates the colocalization between eNOS and different acyl transferases (DHHC-2, -3, -7, and -8). Online supplemental material is available at http://www.jcb.org/cgi/content/full/jcb.200601051/DC1.

This work was supported by grants R01 HL64793, R01 HL 61371, R01 HL 57665, and P01 HL 70295 from the National Institutes of Health to W.C. Sessa. C. Fernández-Hernando is supported by a fellowship from the Spanish Ministry of Education and Science. P.N. Bernatchez is supported by fellowships from the Canadian Institutes of Health Research and the American Heart Association.

Submitted: 20 January 2006
Accepted: 22 June 2006

References

Busse, R., and A. Mulsch. 1990. Calcium-dependent nitric oxide synthesis in endothelial cytosol is mediated by calmodulin. *FEBS Lett.* 265:133–136.

Chaudhary, J., and M.K. Skinner. 2002. Identification of a novel gene product, Sertoli cell gene with a zinc finger domain, that is important for FSH activation of testicular Sertoli cells. *Endocrinology.* 143:426–435.

Degtyarev, M.Y., A.M. Spiegel, and T.L. Jones. 1993. Increased palmitoylation of the Gs protein alpha subunit after activation by the beta-adrenergic receptor or cholera toxin. *J. Biol. Chem.* 268:23769–23772.

Dimmeler, S., I. Fleming, B. Fisslthaler, C. Hermann, R. Busse, and A.M. Zeiher. 1999. Activation of nitric oxide synthase in endothelial cells by Akt-dependent phosphorylation. *Nature.* 399:601–605.

Fukata, M., Y. Fukata, H. Adesnik, R.A. Nicoll, and D.S. Bredt. 2004. Identification of PSD-95 palmitoylating enzymes. *Neuron.* 44:987–996.

Fulton, D., J.P. Gratton, T.J. McCabe, J. Fontana, Y. Fujio, K. Walsh, T.F. Franke, A. Papapetropoulos, and W.C. Sessa. 1999. Regulation of endothelium-derived nitric oxide production by the protein kinase Akt. *Nature.* 399:597–601.

Fulton, D., J.P. Gratton, and W.C. Sessa. 2001. Post-translational control of endothelial nitric oxide synthase: why isn't calcium/calmodulin enough? *J. Pharmacol. Exp. Ther.* 299:818–824.

Fulton, D., R. Babbitt, S. Zoellner, J. Fontana, L. Acevedo, T.J. McCabe, Y. Iwakiri, and W.C. Sessa. 2004. Targeting of endothelial nitric-oxide synthase to the cytoplasmic face of the Golgi complex or plasma membrane regulates Akt- versus calcium-dependent mechanisms for nitric oxide release. *J. Biol. Chem.* 279:30349–30357.

Garcia-Cardena, G., P. Oh, J. Liu, J.E. Schnitzer, and W.C. Sessa. 1996. Targeting of nitric oxide synthase to endothelial cell caveolae via palmitoylation: implications for nitric oxide signaling. *Proc. Natl. Acad. Sci. USA.* 93:6448–6453.

Gordon, J.I., R.J. Duronio, D.A. Rudnick, S.P. Adams, and G.W. Gokel. 1991. Protein N-myristoylation. *J. Biol. Chem.* 266:8647–8650.

Huang, K., A. Yanai, R. Kang, P. Arstikaitis, R.R. Singaraja, M. Metzler, A. Mullard, B. Haigh, C. Gauthier-Campbell, C.A. Gutekunst, et al. 2004. Huntingtin-interacting protein HIP14 is a palmitoyl transferase involved in palmitoylation and trafficking of multiple neuronal proteins. *Neuron.* 44:977–986.

Jagnandan, D., W.C. Sessa, and D. Fulton. 2005. Intracellular location regulates calcium-calmodulin-dependent activation of organelle-restricted eNOS. *Am. J. Physiol. Cell Physiol.* 289:C1024–C1033.

James, G., and E.N. Olson. 1989. Identification of a novel fatty acylated protein that partitions between the plasma membrane and cytosol and is deacylated in response to serum and growth factor stimulation. *J. Biol. Chem.* 264:20998–21006.

Keller, C.A., X. Yuan, P. Panzanelli, M.L. Martin, M. Alldred, M. Sassoe-Pognetto, and B. Luscher. 2004. The gamma2 subunit of GABA(A) receptors is a substrate for palmitoylation by GODZ. *J. Neurosci.* 24:5881–5891.

Li, B., F. Cong, C.P. Tan, S.X. Wang, and S.P. Goff. 2002. Aph2, a protein with a zf-DHHC motif, interacts with c-Abl and has pro-apoptotic activity. *J. Biol. Chem.* 277:28870–28876.

Liu, J., and W.C. Sessa. 1994. Identification of covalently bound amino-terminal myristic acid in endothelial nitric oxide synthase. *J. Biol. Chem.* 269:11691–11694.

Liu, J., G. Garcia-Cardena, and W.C. Sessa. 1995. Biosynthesis and palmitoylation of endothelial nitric oxide synthase: mutagenesis of palmitoylation sites, cysteines-15 and/or -26, argues against depalmitoylation-induced translocation of the enzyme. *Biochemistry.* 34:12333–12340.

Liu, J., G. Garcia-Cardena, and W.C. Sessa. 1996. Palmitoylation of endothelial nitric oxide synthase is necessary for optimal stimulated release of nitric oxide: implications for caveolae localization. *Biochemistry.* 35:13277–13281.

Liu, J., T.E. Hughes, and W.C. Sessa. 1997. The first 35 amino acids and fatty acylation sites determine the molecular targeting of endothelial nitric oxide synthase into the Golgi region of cells: a green fluorescent protein study. *J. Cell Biol.* 137:1525–1535.

Lobo, S., W.K. Greentree, M.E. Linder, and R.J. Deschenes. 2002. Identification of a Ras palmitoyltransferase in *Saccharomyces cerevisiae*. *J. Biol. Chem.* 277:41268–41273.

McCabe, T.J., D. Fulton, L.J. Roman, and W.C. Sessa. 2000. Enhanced electron flux and reduced calmodulin dissociation may explain "calcium-independent" eNOS activation by phosphorylation. *J. Biol. Chem.* 275:6123–6128.

Mumby, S.M., C. Kleuss, and A.G. Gilman. 1994. Receptor regulation of G-protein palmitoylation. *Proc. Natl. Acad. Sci. USA.* 91:2800–2804.

Pollock, J.S., U. Forstermann, J.A. Mitchell, T.D. Warner, H.H. Schmidt, M. Nakane, and F. Murad. 1991. Purification and characterization of particulate endothelium-derived relaxing factor synthase from cultured and native bovine aortic endothelial cells. *Proc. Natl. Acad. Sci. USA.* 88:10480–10484.

Robinson, L.J., L. Busconi, and T. Michel. 1995. Agonist-modulated palmitoylation of endothelial nitric oxide synthase. *J. Biol. Chem.* 270:995–998.

Rocks, O., A. Peyker, M. Kahms, P.J. Verveer, C. Koerner, M. Lumbierres, J. Kuhlmann, H. Waldmann, A. Wittinghofer, and P.I. Bastiaens. 2005. An acylation cycle regulates localization and activity of palmitoylated Ras isoforms. *Science.* 307:1746–1752.

Roth, A.F., Y. Feng, L. Chen, and N.G. Davis. 2002. The yeast DHHC cysteine-rich domain protein Akr1p is a palmitoyl transferase. *J. Cell Biol.* 159:23–28.

Sessa, W.C., C.M. Barber, and K.R. Lynch. 1993. Mutation of N-myristoylation site converts endothelial cell nitric oxide synthase from a membrane to a cytosolic protein. *Circ. Res.* 72:921–924.

Sessa, W.C., G. Garcia-Cardena, J. Liu, A. Keh, J.S. Pollock, J. Bradley, S. Thiru, I.M. Braverman, and K.M. Desai. 1995. The Golgi association of endothelial nitric oxide synthase is necessary for the efficient synthesis of nitric oxide. *J. Biol. Chem.* 270:17641–17644.

Shaul, P.W., E.J. Smart, L.J. Robinson, Z. German, I.S. Yuhanna, Y. Ying, R.G. Anderson, and T. Michel. 1996. Acylation targets endothelial nitric-oxide synthase to plasmalemmal caveolae. *J. Biol. Chem.* 271:6518–6522.

Smotrys, J.E., and M.E. Linder. 2004. Palmitoylation of intracellular signaling proteins: regulation and function. *Annu. Rev. Biochem.* 73:559–587.

Sowa, G., J. Liu, A. Papapetropoulos, M. Rex-Haffner, T.E. Hughes, and W.C. Sessa. 1999. Trafficking of endothelial nitric-oxide synthase in living cells. Quantitative evidence supporting the role of palmitoylation as a kinetic trapping mechanism limiting membrane diffusion. *J. Biol. Chem.* 274:22524–22531.

Swarthout, J.T., S. Lobo, L. Farh, M.R. Croke, W.K. Greentree, R.J. Deschenes, and M.E. Linder. 2005. DHHC9 and GCP16 constitute a human protein fatty acyltransferase with specificity for H- and N-Ras. *J. Biol. Chem.* 280:31141–31148.

Uemura, T., H. Mori, and M. Mishina. 2002. Isolation and characterization of Golgi apparatus-specific GODZ with the DHHC zinc finger domain. *Biochem. Biophys. Res. Commun.* 296:492–496.